ULF Wave Transport of Relativistic Electrons in the Van Allen Belts: Criteria for Transition to Radial Diffusion

Enter authors here: Zhi-Gu Li[1,2], Ian R. Mann[1], Louis G. Ozeke[1], Leonid Olifer[1], and Alexander W. Degeling[1,3]

[1]Department of Physics, University of Alberta, Edmonton, Alberta, Canada.

[2]Department of Physics and Astronomy, West Virginia University, Morgantown, WV, USA.

[3]Shandong Provincial Key Laboratory of Optical Astronomy and Solar-Terrestrial Environment, Institute of Space Sciences, Shandong University, Weihai, China.

Corresponding author: Zhi Gu Li (zhigu.li@mail.wvu.edu)

Key Points:

- We derive analytic expressions required for the transition from coherent to diffusive transport applied to ULF wave-particle interactions
- We characterize the behavior using an equivalent dynamical system model, highlighting the importance of the particle decorrelation time
- For decorrelation times longer than typical ULF wavetrains, particle transport rates cannot be estimated under a radial diffusion paradigm

Abstract

Relativistic electrons in the radiation belts can be transported as a result of wave-particle interactions (WPI) with ultra-low frequency (ULF) waves. Such WPI are often assumed to be diffusive, parametric models for the radial diffusion coefficient often being used to assess the rates of radial transport. However, these WPI transition from initially coherent interactions to the diffusive regime over a finite time, this time depending on the ULF wave power spectral density, and local resonance conditions. Further, in the real system on the timescales of a single storm, interactions with finite discrete modes may be more realistic. Here, we use a particle-tracing model to simulate the dynamics of outer radiation belt electrons in the presence of a finite number of discrete frequency modes. We characterize the point of the onset of diffusion as a transition from separate discrete interactions in terms of wave parameters by using the "two-thirds" overlap criterion (Lichtenberg & Lieberman, 1992), a comparison between the distance between, and the widths of, the electron's primary resonant islands in phase space. Further, we find the particle decorrelation time in our model system with typical parameters to be on the timescale of hours, which only afterwards can the system be modeled by one-dimensional radial diffusion. Direct comparison of particle transport rates in our model with previous analytic diffusion coefficient formulations show good agreement at times beyond the decorrelation time. These results are critical for determining the time periods and conditions under which ULF wave radial diffusion theory can be applied.

Plain Language Summary

The dynamics of Earth's outer Van Allen radiation belt electrons have up to now been almost exclusively modeled using statistical methods. However, such approaches may not be valid for all scenarios. In this work, we defined a criterion separating the regimes where the dynamics of the outer radiation belt electrons can and cannot be modeled statistically, and in particular using a model based around the concepts of diffusion where averaging over many individual interactions leads to an assessment for the overall behavior of a set, or ensemble, of electrons. We use a test particle-tracing model to assess the actual dynamics of particle ensembles when perturbed by a type of plasma waves with ultra-low frequency in space. We showed that there is a distinctive qualitative and quantitative difference between diffusive and the more coherent regimes and identified their point of transition. We further verified that once the system has evolved beyond our derived transition criteria it does indeed match the common statistical predictions, verifying the applicability of a diffusion model after that time. Significantly, however, at earlier times the more correlated system behaves differently and may be characterized by a much faster and coherent transport.

1 Introduction

Relativistic electrons in the outer belt can be transported and energized through the violation of the third adiabatic invariant under drift-resonant interactions with ultra-low frequency (ULF) plasma waves (e.g., Fälthammar, 1965, 1968; Elkington et al., 1999). The storm time enhancements in the flux of these relativistic particles are able to damage the electronics onboard spacecraft passing through the outer radiation belt region, causing costly interruptions in the operations of these satellites, and in the worst-case, total loss (e.g., Baker, 2000). By developing accurate radiation belt models to forecast these flux enhancements, and/or to define worst case radiation environments, many of the impacts of these particles on spacecraft operations might be able to be mitigated (Horne et al., 2013; Reeves et al., 2012; Subbotin et al., 2009; Beutier & Boscher, 1995).

Charged particle interactions with a single ULF wave mode can produce signatures of a coherent resonant process, which transitions towards the diffusive paradigm as the wave frequency spectra become increasingly broadband (e.g., Fälthammar, 1965, 1968; Birmingham et al., 1967; Elkington et al., 1999, 2003; Degeling et al., 2008, 2011). While historically the transport of electrons through interaction with ULF waves is often modeled using the Fokker-Planck equation under the assumption of diffusive dynamics caused by broadband electromagnetic field perturbations (e.g., Davis Jr & Chang, 1962; Schulz & Lanzerotti, 1974), in the real system on the timescales of particle transport during a single storm, interactions with a limited number of discrete modes may be more realistic. This paper attempts to characterize the onset of diffusive behavior by examining the response of the particle ensemble to discrete frequency ULF wave perturbations in a dipole model for the Earth's magnetosphere. Our goal is to establish the conditions for the transition from coherent to diffusive dynamics, and to thereby also determine when these statistical, and specifically diffusive, methods can be properly applied.

Radial diffusion theory first developed by Kellogg (1959), Parker (1960), and Fälthammar (1965, 1968) provided a macro-scale description of radiation belt particle transport and energization mechanisms. A number of major assumptions are required to develop the theory. As a result, disputes occurred arguing the validity of radial diffusion theory, and whether it is applicable to the radiation belt environment. For example, Riley & Wolf (1992) showed only moderate correlation between test-particle simulations and radial diffusion theory, while Ukhorskiy et al. (2006) argued that the theory itself could be ill-posed as the fundamental physical process is not diffusion. Presently, the mechanisms of radiation belt particle transport and energization are not completely understood, and a number of efforts have been made to unify the test-particle results, radial diffusion theories, simulation results, and observational data. In the work presented here, we return to the question of reconciling results from the single particle tracing and radial diffusion paradigms.

Important work on particle-tracing models and transport mechanisms completed by Elkington et al. (1999, 2003) studied the effects on particle ensembles when they resonate with discrete frequency ULF waves. With reference to the Chirikov resonance overlap criterion (Chirikov, 1979), and the "two-thirds" resonance overlap rule (Lichtenberg & Lieberman, 1992), which must be satisfied in order for a resonant dynamical system to transition to show diffusive behavior, Elkington et al. demonstrated that their simulated ensemble of test particles exhibited behavior that closely matched estimates of the radial transport rates derived from radial diffusion theory. We expand on their work by closely examining this stochastic transition as the "two-thirds" overlap rule is satisfied for multiple mode ULF wave-particle interactions in a single-particle tracing model. Specifically, we show that in order to demonstrate diffusive behavior, the system has to evolve for a sufficiently long timescale for it to go from a correlated to a decorrelated state (Lichtenberg & Lieberman, 1992). Degeling et al. (2011) found in his test-particle models that the typical correlation decay time is on the order of 10-15 wave periods, which is comparable to the length of the wavetrains for ULF waves observed in geospace. We further investigate this phase decorrelation process in conjunction with multiple wave modes separated in frequency and the "two-thirds" resonance island overlap criterion and derive an analytic criterion for the timescale for this transition from coherent to diffusive behavior.

Specifically, we trace particles in a wave model which comprises a number of discrete frequency ULF modes, and whose frequency separation can be used to assess this transition. Our model is designed to allow investigation of the combined effects of mode frequency spacing, wave amplitude, and the importance of the particle decorrelation time. We further analyze the wave-particle dynamics using an analogue dynamical system model, and estimate the time required for the particle ensemble to become decorrelated. Overall, we show how these criteria correctly estimate the point of the transition to stochastic behavior and further show therefore how it defines the timescale only beyond which radial diffusion models can be appropriately applied to ULF wave-particle interactions in the radiation belts.

2 Model

We take the approach of using a single particle-tracing method to track the guiding center position of individual electrons in a given ensemble for a period of time t. We adopt a symmetric dipole background magnetic field and model the effects of multiple discrete frequency ULF disturbances on the ensemble electron dynamics. To simplify the approach, we use a 2-dimensional particle-tracing model and focus on equatorial particle dynamics. The ULF waves are modeled as Alfvénic disturbances, which are further assumed to be fundamental field-aligned modes, locally standing field line resonances. Finally, we use this model to simulate ensemble particle dynamics, and compare the results to empirical criteria to be defined in Sections 4 and 5, which indicates the separation between the initial epoch of coherent behavior, and the later stochastic and diffusive dynamical behavior.

2.1 Particle Tracing Model

For a single charged particle, the first order guiding center drift equations in spherical coordinates were originally derived by Northrop (1963), and can be simplified for equatorial particles to (Degeling et al., 2008):

$$\dot{L} = \frac{E_\phi}{BR_E} - \frac{\mu}{q\gamma LBR_E^2}\frac{\partial B}{\partial \phi}, \#(1)$$

$$\dot{\phi} = -\frac{E_r}{LR_EB} + \frac{\mu}{q\gamma LBR_E^2}\frac{\partial B}{\partial L}. \#(2)$$

Here, E_r and E_ϕ are the radial and azimuthal components of the wave electric field respectively. Further, B is the local scalar magnetic field strength, μ is the particle's first adiabatic invariant, q is its electric charge, and γ is the relativistic Lorentz factor. L is the L-shell parameter describing a particular set of planetary magnetic field lines (McIlwain, 1961). The first adiabatic invariant for an electron is defined as

$$\mu = \frac{p_\perp^2}{2m_eB} , \#(3)$$

where $p_\perp$, is the electron's momentum perpendicular to the background magnetic field and m_e is the electron mass. For ULF wave interactions, μ is assumed to be conserved since the characteristic time of the field variations are slow compared to the gyration period of the particle (e.g., Schulz & Lanzerotti, 1974; Ukhorskiy & Sitnov, 2012).

The Lorentz factor for electrons in the equatorial plane can be expressed as

$$\gamma(B) = \sqrt{\frac{2\mu B}{m_e c^2} + 1}, \#(4)$$

where c is the speed of light in a vacuum. A 4$^{\text{th}}$-order Runge-Kutta routine is used to integrate equations (1) and (2) to obtain the electron's guiding center motion in the equatorial plane. While an asymmetric field model may be more representative of reality, we argue that the underlying physics of a transition from a regular to stochastic regime will be similar in view of the "two-thirds" overlap criterion. We therefore adopt an axisymmetric dipole for simplicity, and for ease of deriving the structure of the equatorial electric fields of the ULF waves. The axisymmetric scalar magnetic field strength is then given by

$$B(L) = \frac{B_0}{L^3}, \#(5)$$

where B_0 is the magnetic field measured on Earth's equatorial surface, 31.2 μT.

2.2 ULF Wave Model

In this work, we analyze the particle ensemble characteristics under the effects of Alfvénic ULF wave disturbances. We choose an MHD Alfvén wave field corresponding to an isolated field-aligned standing field line resonance (which does not compress the plasma, such that the parallel magnetic field perturbation is zero) and which satisfies the condition $\nabla \times \boldsymbol{E} = 0$. We only consider particle motion in the equatorial plane; we consider fundamental field-aligned modes, such that this mode only has perpendicular electric field perturbations in the equatorial plane, with a node in the perpendicular magnetic components. Further, this narrows our study to only one diffusion mechanism due to electric wave perturbations.

Here, we implement ULF modes with a finite width envelope in L, with a Gaussian amplitude profile centered on a given L_0, with a half-width σ. Further, a constant phase off-set, Φ_0, is assigned to each individual frequency mode, where this phase off-set is randomly determined at the initial time between 0 and 2π. Additionally, a constraint is imposed on the ULF waves dictating that the wave phase must not maintain total coherence and a constancy of phase across multiple Ls, consistent for example with either phase lags from the propagation of an assumed driver across L, or due to the L-dependent phase which develops in driven field line resonance solutions (e.g., Southwood, 1974). A valid ansatz is to implement this L-dependent phase advance by inserting a $2\pi L/\zeta$ phase factor, where ζ characterizes the rate of change of oscillation phase in relation to L. Under these constraints, the radial electric field can be derived from an assumed analytic form of the azimuthal electric field in accordance with $\nabla \times \boldsymbol{E} = 0$. We further assume azimuthally propagating modes, with an azimuthal phase speed defined by the ratio of the wave angular frequency, ω, and the azimuthal wavenumber, m, such that:

$$E_0(L) = A \exp\left[-\frac{(L-L_0)^2}{2\sigma^2}\right], \#(6)$$

$$\Delta(L) = \tan^{-1}\left[\frac{\zeta}{2\pi\sigma^2}\frac{L(L-L_0)-\sigma^2}{L}\right], \#(7)$$

$$E_r = \frac{E_0(L)}{m}\sqrt{\left(\frac{2\pi}{\zeta}L\right)^2 + \left(L\frac{L-L_0}{\sigma^2} - 1\right)^2}\cos\left[m\phi - \omega t + \Phi_0 + \frac{2\pi}{\zeta}L + \Delta(L)\right], \#(8)$$

$$E_\phi = E_0(L)\cos\left[m\phi - \omega t + \Phi_0 + \frac{2\pi}{\zeta}L\right], \#(9)$$

where $E_0(L)$ is the Gaussian amplitude profile, σ is the Gaussian half width, $\Delta(L)$ an additional L-dependent phase factor resulting from the $\nabla \times \boldsymbol{E} = 0$ condition, and A is the amplitude measured at the peak of the Gaussian profile (at $L = L_0$). The azimuthal wavenumber of the ULF wave, m, such that positive values correspond to the wave propagating eastwards (e.g., Southwood et al., 1969).

Equations (8) and (9), in combination, give rise to one discrete frequency mode, $\boldsymbol{E}(\omega) = E_r\hat{\boldsymbol{r}} + E_\phi\hat{\boldsymbol{\phi}}$, with components pointing in the radial and azimuthal directions respectively. Numerous discrete frequency modes are created through the superposition of individual modes. The model varies L_0, ω, and Φ_0 between individual modes, while σ, m, and ζ are kept constant. The values of these constants are chosen to be $\sigma = 0.5$, $m = 20$, and $\zeta = 1$, where the value of $\zeta = 1$ dictates that the phase advances at a rate of 2π per unit L.

Notably, while ζ does play a role in the effective amplitude of E_r, it does not affect the net rate of radial transport of the particles. This is because, the rate of change of energy, dW/dt, of a charged particle due to a wave electric field, $\boldsymbol{E}$, is given by

$$\frac{dW}{dt} = q\boldsymbol{E}\cdot\boldsymbol{v_d} = q\boldsymbol{E_\phi}\cdot\boldsymbol{v_{GC}},$$

where $\boldsymbol{v_d}$ is the particle's first-order drift velocity vector and $\boldsymbol{v_{GC}}$ is the particle's drift velocity due to gradient-curvature drift, see equations (1) and (2). Note that for equatorially mirroring particle trajectories in the equatorial plane, only the gradient drift is active. Moreover, we assume that there is no background convection electric field. Since $\boldsymbol{E}\cdot(\boldsymbol{E}\times\boldsymbol{B})$ is trivially zero, the particle's *E-cross-B* drift will not in any case contribute to the particle's change in energy. Consequently, E_r does not directly affect the particle's rate of change of energy in the axisymmetric dipole background magnetic field. For these highly relativistic electrons, the gradient drift speed is much larger than the *E-cross-B* speed, such that any resonance island distortion effects arising from E_r (e.g., Degeling et al., 2019) are also negligible. This was further confirmed in simulation, and as a partial test of the particle trajectory integration code (not shown).

3 Results: ULF Wave-Particle Interactions

In order to examine the characteristics of the ULF wave-particle interactions, we examine the dynamics of an initial distribution of particles with the same first adiabatic invariant under the action of the wave electric field. For equatorial charged particles in an axisymmetric background dipole magnetic field, the drift resonance condition can be expressed as

$$\omega = m\omega_d, \#(10)$$

where ω_d is the particle's angular drift frequency, with positive chosen to be eastwards by convention (e.g., Southwood et al., 1969). Equation (10) is used to determine the electron's resonant energy, which by equation (3) gives the electron's resonant location in L, required for a given ULF wave mode with angular frequency ω, and wavenumber m.

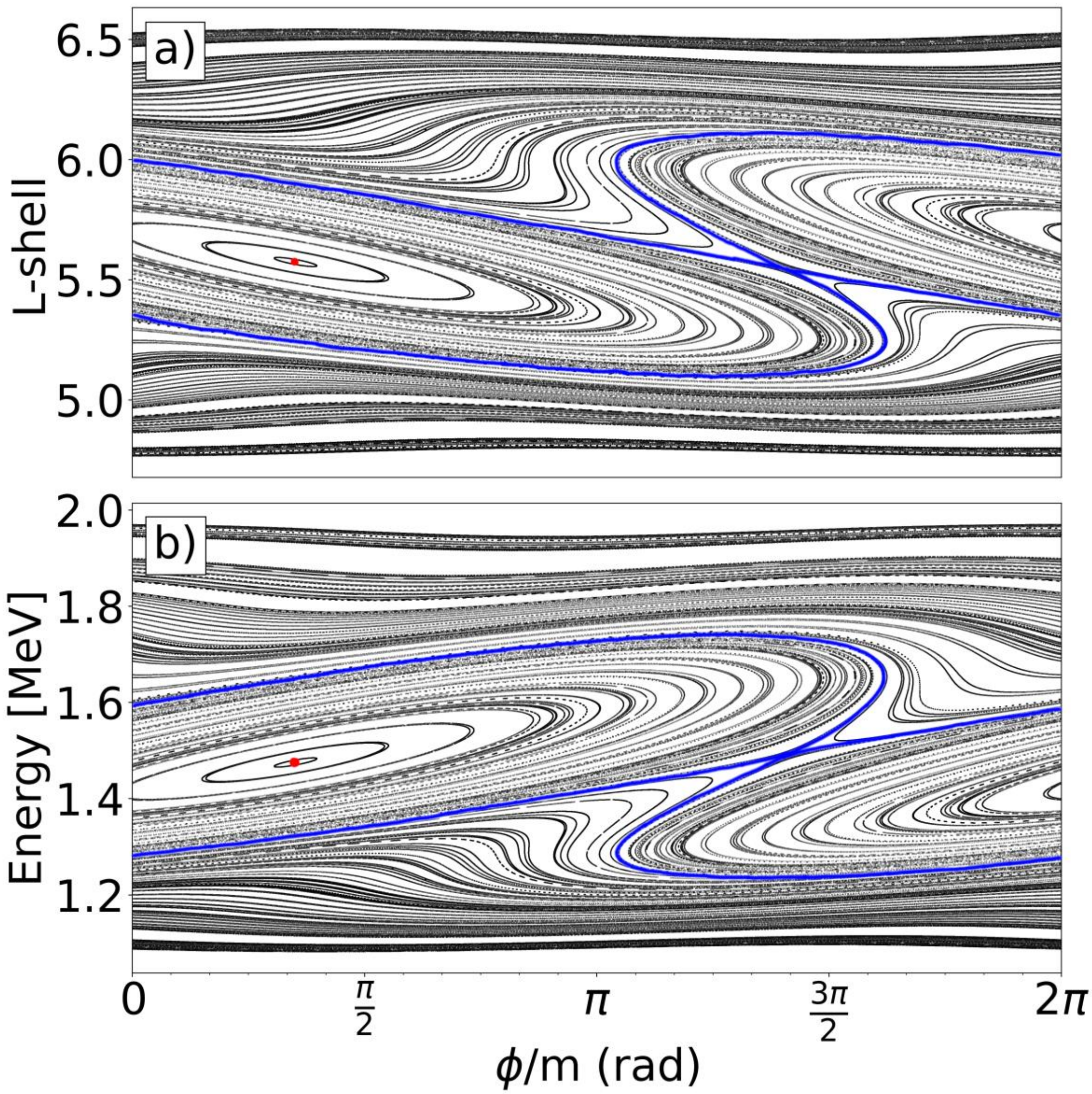

Figure 1. Stroboscopic Poincaré map demonstrating equatorial drift-resonant interactions between electrons and a single ULF mode on the equatorial plane. Panel (a) demonstrates both the resonant and non-resonant electrons interacting with the oscillation mode in L and panel (b) shows the same interaction in terms of electron kinetic energy. The red dot represents the center of the resonant island where the particle's L or energy satisfies equation (10), and the blue contour corresponds to the phase space separatrix.

Both drift resonant and non-drift resonant wave-particle interactions can be visualized on a Poincaré map. Figure 1 shows a Poincaré map for the interaction of a single ULF wave mode, with a frequency of 39 mHz, and $m = 20$, and a collection of 160 electrons which are initially evenly distributed between $L = 4.9$ and $L = 6.5$, and in azimuth. Resonant particles move around in phase space in response to the wave electric field, producing a closed (bound) orbit of the *libration* type. On the other hand, the non-resonant particles do not exhibit such behavior and form unbounded trajectories in phase space of the *rotation* type (e.g, Goldstein et al., 2002). The separatrix determines the boundary separating these two types of behavior as shown by the blue contour in Figure 1. Figure 1 is a special case of a Poincaré map, known as a stroboscopic map (Lichtenberg & Lieberman, 1992). In a stroboscopic map such as that shown in Figure 1, each point is plotted at specific increments in time which are a constant fraction of the wave oscillation period corresponding to a wave phase increment of 2π. This can be compared to the standard plot of trajectories in the frame moving with the wave, where locations in phase space can be plotted at arbitrary time intervals (see e.g., Figure 10 of Loto'Aniu, et al., 2006).

The collection of bound orbits produced by a resonant wave-particle interaction is often referred to as a *resonant island* (see e.g., Lichtenberg & Lieberman, 1992; Elkington et al., 2003). The widths of these islands are determined by the local amplitudes of the wave, and larger amplitudes correspond to an increase in the trapping width of particles in L (and also in energy). The center of these resonant islands is governed by the resonance condition where equation (10) is satisfied. The resonant island center for each individual wave mode is used in determining their respective L_0 in equations (6), (7), and (9) to maximize the resonant wave-particle interactions. In our simulations, all the electron dynamics are examined at $\mu = 2000$ MeV/G, which corresponds to 1 to 4.5 MeV electrons between $L = 7$ and $L = 3$.

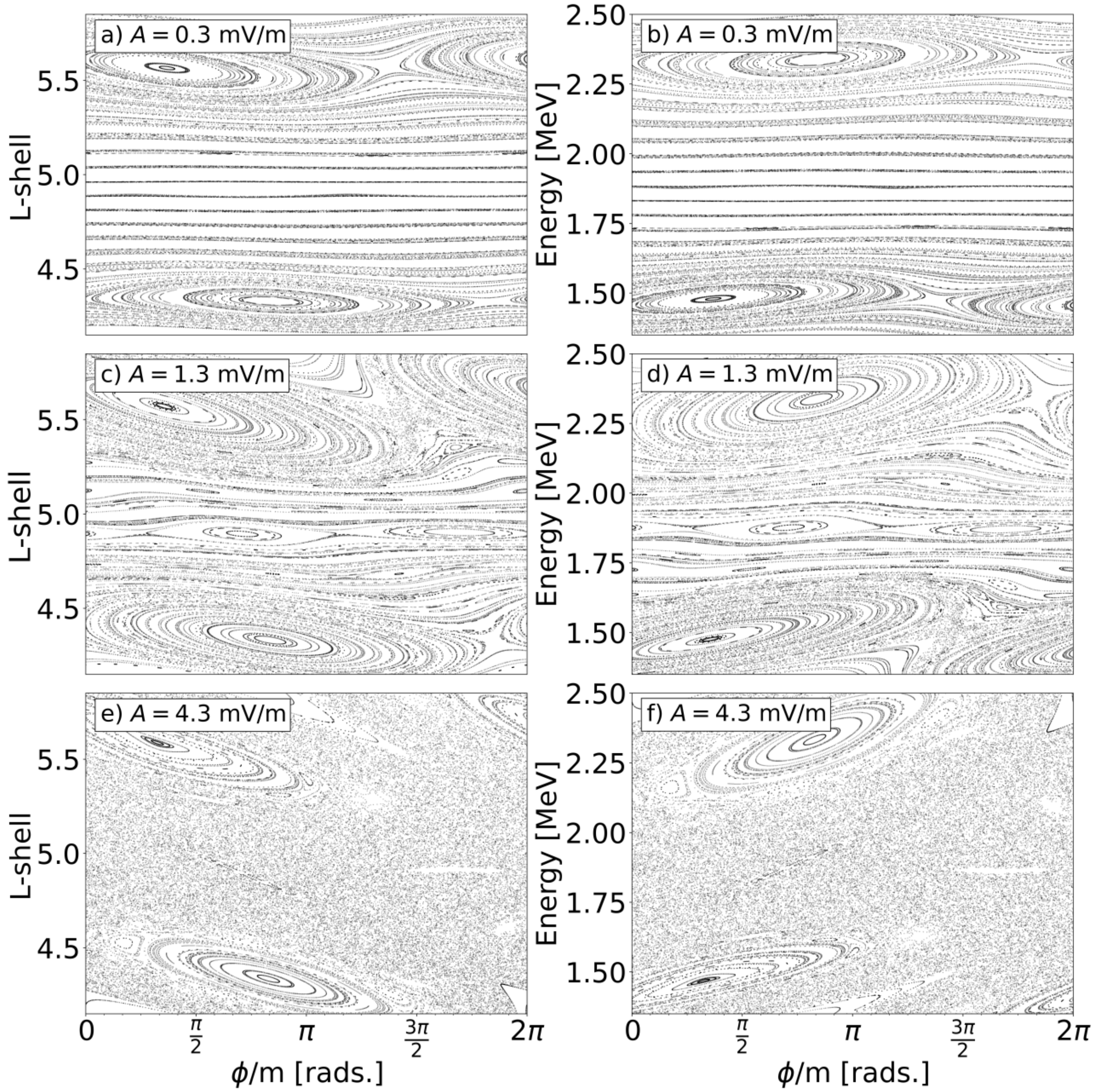

Figure 2. A series of stroboscopic Poincaré map demonstrating the effects of increasing wave amplitude on a system of two resonant modes, $f = 39$ mHz, and $f = 45$ mHz. Panels (a) and (b) corresponds to a wave amplitude of $A = 0.3$ mV/m for both resonant modes, producing largely coherent wave-particle interactions. Panels (c) and (d) are subjected to a wave amplitude of $A = 1.3$ mV/m for both modes and are beginning their transition to diffusion through the creation of various higher order resonant islands. Lastly, panels (e) and (f) are under the effects of two resonant modes both with amplitudes $A = 4.3$ mV/m. See text for details.

An important consideration for the transition from coherent to diffusive dynamics is the separation and potential overlap of the resonant islands in phase space, for example through the 'two-thirds' overlap criteria. The advantage of using a stroboscopic map is that it allows for the visualization of coherent wave-particle interactions in the presence of numerous wave modes with different discrete frequencies. When multiple resonance conditions are satisfied for an ensemble of particles of the same $\mu = 2000$ MeV/G, one can examine the transition to stochastic particle transport, which can be characterized as a diffusive process, as a function of the wave magnitude. Figure 2 demonstrates the particle resonance structures in phase space in response to two ULF electric field wave modes with frequencies 39 and 45 mHz, with $m = 20$, as a function of amplitude. Figure 2a and 2b shows well-defined structures which are indicative of two separate coherent resonant island interactions when $A = 0.3$ mV/m. However, with increasing electric field amplitude, the primary resonant islands grow in size, causing the birth of secondary resonant islands, and distortions along the edges of the previously well-defined single resonance island phase space orbits (cf. Figure 2c and 2d). Furthermore, a stochastic sea forms in the regions between the primary and secondary islands as the wave amplitudes are increased further (cf. Figure 2e and 2f). This interference between the adjacent wave mode frequencies is what causes the transition from a coherent interaction of individual resonant islands, into behavior indicative of a transition to, or the onset of, diffusion within the system.

4 Defining an Analytic Condition for the Transition to Radial Diffusion

As shown in Section 3, when the wave amplitude is sufficiently large, the phase space of the electron dynamics transition from being coherent to largely stochastic, a diffusive region in the phase space being created as a result of the interactions between formerly distinct resonance islands. In general, there exists a region of stochastic behavior for any near-integrable systems (integrable systems with small perturbations), and which is most often located exterior to the primary resonant islands. This region is highly sensitive to initial conditions and grows in size with increasing perturbation amplitude as shown in Lichtenberg & Lieberman (1992). Once this stochastic region dominates the phase space of the dynamical system, the system is considered to have transitioned into global stochasticity. Here, we propose to define an analytic condition which corresponds to a physical realization of this transition, and which is defined in terms of the primary resonant island widths and their spatial separations in phase space. In order to define this transition point, we adopt the “two-thirds” overlap rule commonly referenced in statistical theory (e.g., Lichtenberg & Lieberman, 1992) such that:

$$\kappa_{ij} = \frac{\delta L_i + \delta L_j}{\left|L_{0i} - L_{0j}\right|} \geq \frac{2}{3}, \#(11)$$

where L_{0i} and L_{0j} are the center locations of the two primary islands of interest. Further, δL_i and δL_j are their respective resonance island half-widths as measured independently and assuming no influence from the other. These quantities are used to calculate κ_{ij} which is our transition criterion, where above the threshold, $\kappa_{ij} \approx 2/3$, the system transitions into global stochasticity (in our case radial diffusion) resulting from the merging of adjacent resonant islands. This criterion only governs the region between the i-th and j-th resonant frequencies and the term “global” refers to the region of L between the resonant island centers corresponding to these two resonant frequencies.

In the example shown in Figure 2, which demonstrates this transition to global stochasticity, it is clearly seen that further increases of wave amplitude beyond the onset of diffusion lead to further growth of the size of the stochastic region. At the same time, the size of the remnant primary resonant islands shrinks. Because the shrinking islands will continue to trap particles, producing periodic particle motion rather than diffusive transport, this ultimately causes the particle ensemble behavior to deviate away from that of ideal one-dimensional diffusion. The effects of these long-lasting and vestigial islands can be reduced by implementing additional oscillation modes, introducing more scattering into the dynamical system, or by further increases in wave amplitudes. This is because, while the independently measured island half-width increases with perturbation strength, the half-width of an island under interference contrarily decreases as the system becomes progressively more stochastic (compare, for example, Figure 2c with 2e).

The primary resonant island for a given resonant wave mode is centered in L where the drift resonance condition is satisfied. This location can be determined by implicitly solving equation (2) under the constraint of equation (10). Approximately, the solution can be explicitly expressed as

$$L_0(\omega) \approx \Lambda^{1/3}\left[\left(1+\sqrt{1+\eta\omega^6}\right)^{1/3} + \left(1-\sqrt{1+\eta\omega^6}\right)^{1/3}\right], \#(12)$$

$$\text{where} \quad \Lambda = \frac{\mu B_0}{m_e c^2}, \qquad \text{and} \qquad \eta = \frac{2^6}{3^9}\left(\frac{B_0 R_E^3}{m_e c^2}\right)^4 \frac{q^6}{m^6 \mu^2},$$

where the constants Λ, and η are used to bring equation (12) into a condensed form. Equation (12) is derived utilizing an approximation that equation (4) can be described accurately by its first order Taylor expansion for relativistic electrons and its full derivation can be found in Appendix A. Furthermore, the independent resonant island half-width can also be approximated under the same condition as used to derive equation (12), which also assumes the effect of *gradient* drift to dominate *E-cross-B* drift in the particle's azimuthal motion, and the additional requirements that the perturbation strength is assumed to be small and constant across the domain of the resonant island. Given that $L_0 \gg \delta L$ and following a similar derivation found in Degeling et al. (2007), the independent resonant island half-width can be explicitly expressed as:

$$\delta L \approx \sqrt{\Gamma E_0(L_0)\frac{L_0^{4.5}}{1+QL_0^3}}, \#(13)$$

$$\text{where} \quad \Gamma = \sqrt{\frac{32 q^2 R_E^2}{9 B_0 \mu m_e c^2 m^2}}, \qquad \text{and} \qquad Q = \frac{5 m_e c^2}{4\mu B_0},$$

where again, the constants Γ and Q are used to bring equation (13) to a more condensed form. The full derivation can be found in Appendix B.

The advantage of equations (12) and (13) is that they allow us to express our transition criterion in terms of only wave properties, such that the criteria $\kappa_{ij} = \kappa_{ij}(E_0, \omega)$. By knowing various wave properties such as wave amplitude, frequency, azimuthal wavenumber, and storm time region, we can infer whether a group of electrons with specific values of μ are expected to demonstrate dynamical behavior which can be characterized as radial diffusion. The regions where the resulting radial diffusion occurs depends on the domain where equation (11) is satisfied. As an example, for 3 resonant wave modes assigned i, j, and k, and where the primary resonance island of j is situated between those of i and k, if the criteria for κ_{ij} and κ_{jk} being greater than 2/3 are both satisfied, only then can a particle be diffusively transported through the entire region from $L_0(\omega_i)$ to $L_0(\omega_k)$. Otherwise, if the criterion is satisfied for only one pair of the two quantities, then particle transport will be limited to, and only occur in regions between, the pair of resonant modes that satisfies equation (11). Therefore, the resonant island overlap quantity κ_{ij} must not be less than 2/3 between each adjacent wave frequency pair for the electron dynamics to become diffusive throughout the entire domain where the waves are present. Furthermore, this can be generalized to a system with an arbitrary number of discrete wave frequencies, N, where the two-thirds overlap criterion for each adjacent wave pair can be computed.

This approach is illustrated in Figure 3. For example, in Figure 3a, the value of κ_{ij} is calculated for a system of $N = 19$ wave modes, and which span a frequency range from 37.5 mHz to 46.5 mHz, with a frequency spacing, $\Delta f = 0.5$ mHz. The value of κ_{ij} is only calculated for pairs of neighboring frequencies, L is determined to be the average between the pair of resonant island locations, L_{0i} and L_{0j} Panel (b) illustrates the minimum amplitude required in order to satisfy the two-thirds overlap criterion in equation (11) as a function of the frequency separation of adjacent modes, Δf.

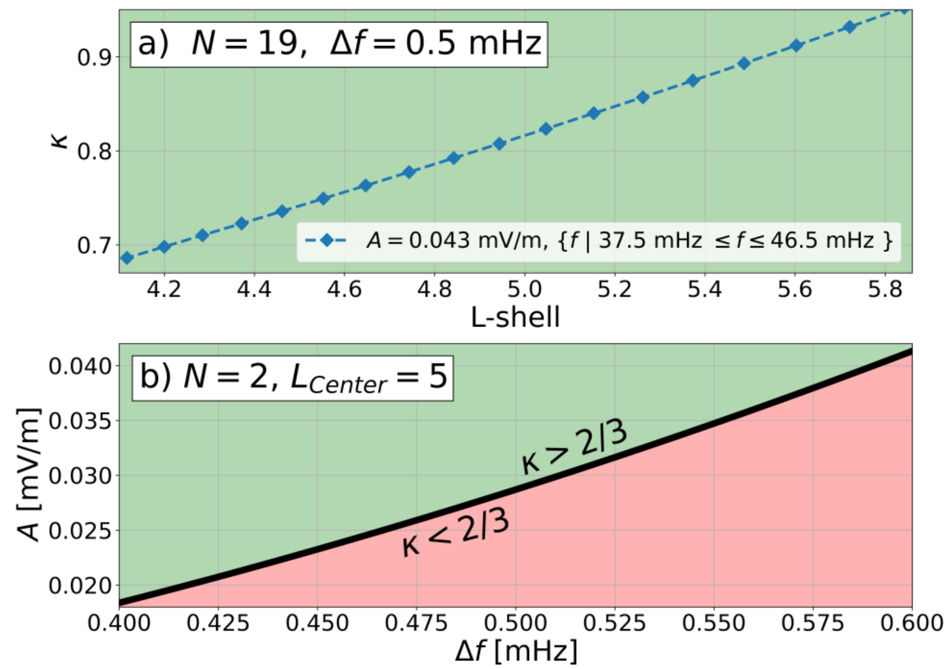

Figure 3. (a) Solutions for κ_{ij} for a system of 19 discrete frequency wave modes all with amplitude $A = 0.043$ mV/m. (b) Shows the minimum wave amplitude needed to satisfy equation (11) as the frequency spacing and amplitude is varied, for only a pair of wave modes where the average of the 2 electron resonant island centers is located at $L = 5$. The background color indicates where κ_{ij} is above (green) or below (red) the criteria of 2/3. See text for details.

Specifically, Figure 3b shows this criterion for two wave modes situated near $L \approx 5$. Demonstrated by Figure 2 and 5b, the wave power and the proximity of adjacent mode frequencies plays a key role for the onset of diffusion, and for the ability of the perturbing waves to create diffusive transport in these wave-particle interaction systems. This result agrees with analyses which assess dynamics on terms of the wave perturbations' power spectral density (PSD), present in most analytical radial diffusion theories (see e.g., Fälthammar, 1968; Fei et al., 2006; Lejosne, 2019), due to its ability to capture both the wave amplitude and frequency separation information of the perturbations.

5 Characteristics of the Transition to Radial Diffusion: Analytical and Numerical Assessments

In this section we use numerical and analytical approaches to calculate the radial diffusion coefficients for our wave-particle interaction system. We now examine a system containing 19 discrete frequency modes to demonstrate the general applicability of the two-thirds overlap criterion. The radial diffusion coefficients can be characterized by the average ensemble deviation of the electrons from their initial starting position over a time scale τ (e.g., Elkington et al., 2003; Lejosne, 2019),

$$D_{LL} \equiv \frac{\langle \Delta L^2 \rangle}{2\tau}, \#(14)$$

where D_{LL} is the radial diffusion coefficient, and $\langle \Delta L^2 \rangle$ is the square of the particles' deviation from their initial position averaged over the entire ensemble.

As mentioned previously in Section 4, diffusive stochastic behavior can arise from the interference between only two primary resonant islands (cf. Figure 2). However, in this case the diffusion only occurs in limited regions of phase space near and between the primary resonance islands. Further, even following the transition to diffusion electrons trapped close to the remnant resonant islands radially oscillate about the center of the resonant island and therefore undergo no net radial transport. As compared to a system where particles are able to freely diffuse over all regions of phase space, the remnant resonant islands within our model can be expected to impede the overall growth of $\langle \Delta L^2 \rangle$ in time. Because the radial diffusive transport of the particles takes place only near the vicinity of overlapping resonant islands, there must exist a transport boundary where no resonant islands are situated on the exterior. Hence, for a narrow band of discrete frequency waves, the particle transport is confined within the resonant region where the boundary is determined by the locations of the islands corresponding to the outermost resonant frequencies.

The domain of our numerical simulation is chosen to range from $L = 4$ to $L = 6$, and particles drifting beyond this region are removed from the simulation. This narrow domain allows for the study of local D_{LL} characteristics, and in what follows we examine the dynamics at the center of the domain at $L \approx 5$. For ULF waves with $m = 20$ to be resonant with $\mu = 2000$ MeV/G electrons in our domain, equation (10) dictates ULF waves spanning frequencies from 37.5 to 46.5 mHz. A finite number of ULF wave modes with discrete frequencies spanning this frequency range are chosen, with a narrowly spaced $\Delta f = 0.5$ mHz corresponding to $N = 19$ discrete modes with a comb-like frequency spectrum. The close frequency separation in combination with the wide Gaussian wave amplitude width, $\sigma = 0.5$, allows for an approximately locally constant wave PSD of $P = A^2/2\Delta f$ (Elkington et al., 2003). Furthermore, the PSD can be equally estimated through Fourier methods (see e.g., Welch, 1967), where both methods have been confirmed to yield very similar results (not shown). Finally, 7200 particles are distributed randomly in azimuth along a constant ring at $L = 5$, where they are allowed to interact freely with the prescribed wave field and the time evolution of their positions are recorded. Since the initial wave phase of each mode, and each particle's azimuthal position, are both randomized, several runs of different initial randomizations are averaged to produce final results where we can be confident that any artifacts that arose from the initial conditions have been averaged out.

A system starting in an initial state of order can transition into a disorderly state through these multiple resonant wave-particle interactions. Under the right conditions, the motion of the particles in the disordered state can behave stochastically, similar to that for Brownian motion due to collisions, and their long-term evolution therefore described by statistical methods. However, unlike these collisional gaseous systems, here the particle interactions are collisionless with the resonant wave-particle interactions with multiple ULF waves providing the basis through which the particles within the ensemble interact in a way analogous to random collisions. This suggests that a disorderly transition requires the existence of a non-negligible correlation decay time τ_c (CDT) such that only after τ_c can the system behave stochastically. This suggests that the particles start their dynamics in a correlated state, and through ULF wave-drift resonant interactions, they would initially undergo phase mixing as the particles respond to the perturbing wave fields. In the case of a *kick rotator*, the CDT can be estimated by (e.g., Zaslavsky, 2002; Ukhorskiy & Sitnov, 2012):

$$T = \frac{1}{\Delta f}, \#(15)$$

$$\tau_c = \frac{2T}{\ln K}, \#(16)$$

where T defines the time interval of these "collisions" experienced through resonant wave-particle interactions, and K is a characteristic non-linearity factor of the system. Equation (16) is valid given that K is sufficiently large ($K \gg 1$). The non-linearity factor K, is often referenced in statistical theory and is directly related to the phase space structures found in the dynamics such as those shown in Figure 2 (see e.g., Chirikov, 1979; Lichtenberg & Lieberman, 1992; Zaslavsky, 2002). Ukhorskiy & Sitnov (2012) proposes that for similar alternative systems, the CDT, τ_c, should still follow the same functional dependence of equations (15) and (16). We hypothesize that, for our model, the characteristic "collision" time T should still be inversely proportional to the wave mode frequency spacing, and the non-linearity parameter K should scale with wave amplitude and frequency spacing. Hence, an ansatz is formed of similar form to equations (15) and (16) containing two proportionality constants, p_1 and p_2:

$$T = \frac{p_1}{\Delta f}, \#(17)$$

$$K = p_2 \frac{A}{\Delta f^2}, \#(18)$$

$$\tau_c = \frac{2p_1}{\Delta f \ln\left(\frac{p_2 A}{\Delta f^2}\right)}, \#(19)$$

where p_1 and p_2 are determined via best-fit in our model. The derivation of proportionality for K in a dynamical system of resonant ULF wave-particle interactions relativistic electrons follows a similar approach to that in Ukhorskiy & Sitnov (2012) and is detailed in Appendix C. Equation (19) serves as an important ansatz which can be tested in our simulations to verify its ability to correctly predict the CDT in our model.

In our model, in the early time period of the wave-particle interactions, the particles are rapidly dispersed away from their initial position due to the sudden turn-on of the electric field perturbations. After a period, τ_c, the particles have been appropriately phase-mixed such they then exhibit the behaviors of a stochastic system characterized by a diffusion coefficient, given by equation (14), which approaches a constant value (Lichtenberg & Lieberman,1992; Degeling et al., 2007, 2011). Text and Figure S1 of Supporting Information demonstrates that the onset of global particle transport is independent of the rate at which the electric field perturbation grows from 0 mV/m, and within the stochastic regime, particle transport rates are unaffected. However, the CDT is amplitude dependent. Therefore, in this work, we restrict our study of the CDT to the case where the electric field is instantaneously turned-on, and the amplitude (A) remains constant throughout the duration of each simulation.

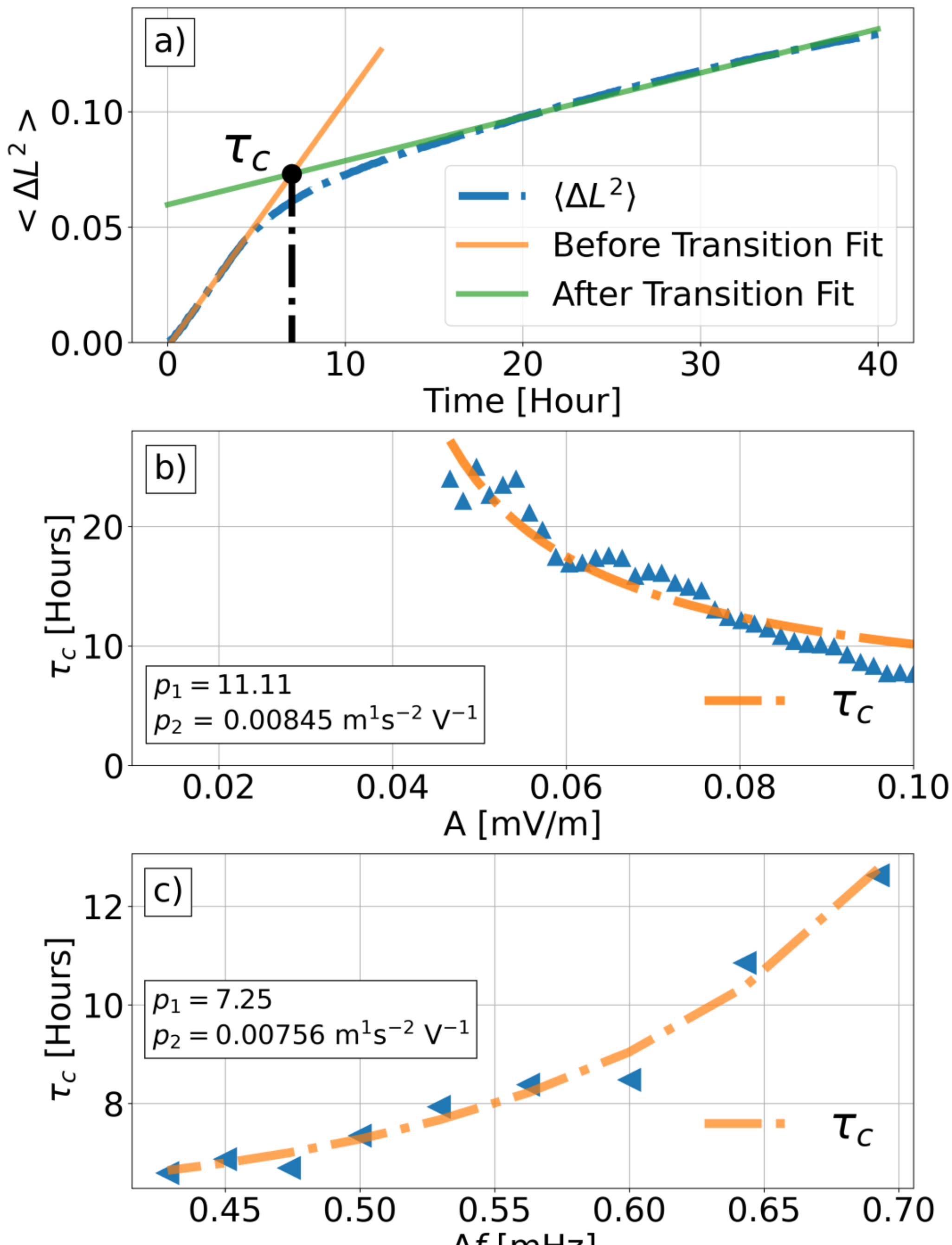

Figure 4. (a) Ensemble $\langle \Delta L^2 \rangle$ as a function of time. Here, a system of 7200 electrons is simulated for 40 hours; 19 discrete ULF wave modes are evenly spaced in frequency from 37.5 to 46.5 mHz, each mode with a constant amplitude $A = 0.1$ mV/m. The intersection of the two linear lines fitted onto the initial and later times is what we hypothesize to be the basis for estimated the CDT, τ_c. (b) and (c) Estimates of the derived τ_c as a function of A (with constant $\Delta f = 0.5$ mHz) and Δf (with constant $A = 0.1\, mV/m$), respectively. For the simulations in panel (c) the same fixed overall frequency range is evenly divided with 14 to 25 modes, each run therefore being spaced with different Δf. The right region of panel (b) follows the predicted trend of equation (19) while the left region contains amplitudes that are unable to be resolved

within the 40 hours of the simulation time window and are therefore excluded from the fit. The resulting parameterization for the CDT, τ_c, arising from the ansatz and model in equations (19) is overplotted in panels (b) and (c).

The characteristics of coherent and stochastic dynamical regimes, and the transition between them, are identifiable by examining the ensemble evolution of $\langle \Delta L^2 \rangle$. Figure 4a demonstrates a gradual transition between the initially coherent motion, which characterizes a faster rate of transport compared to radial diffusion (as it will become apparent in Section 6), and the complete stochasticity of the later phase dynamics. The initial rapid dispersion of the particle ensemble lies in stark contrast to the ensemble transport rates seen at later times. The initial dynamics are characterized by a larger slope in the ensemble $\langle \Delta L^2 \rangle$ as a function of time, and it is this distinction that will be used to estimate the CDT of our system using the results from numerical simulations. We hypothesize that the CDT can be estimated in the numerical simulations as lying in the vicinity of this transition between these two states. Further, we take the approach that the CDT can be estimated as the time of intersection between two approximately linear regimes defining the early coherent and latter stochastic regimes in plots of ensemble $\langle \Delta L^2 \rangle$ in time. This approach is illustrated in Figure 4a, and where lines fitted onto the early and later stages of evolution intersect to provide an estimate of the CDT of the system. Although this approach to estimating τ_c requires extrapolation into the transition region from the coherent (early) and stochastic (later) regimes, it provides an approach to quantify an estimate for CDT, and through which the ansatz for this dynamical system presented above can be assessed. For example, Figures 6b and 6c demonstrate that the τ_c estimated using this method does in fact follow the expected proportionality to A and Δf as predicted by equation (19). Therefore, for our intents and purposes, we consider τ_c derived in this way to represent a viable method for its estimation.

The range of simulation time intervals for the two linear fits used to calculate τ_c are in the range of 1 to 3 hours, and 25 to 40 hours, for the initial (correlated) and latter (diffusive) regions. The first hour of simulation time was excluded from the estimate of the initial $\langle \Delta L^2 \rangle$ time evolution to allow for all particles to interact with all wave modes for the initial few wave periods. Also note that for most of the simulation runs, the transition to diffusion occurs well-within 25 hours. This becomes important later in Figure 6 as it dictates the wave mode amplitudes needed in order to be able to observe the system transition into the diffusive regime in a 40-hour simulation.

The numerical results shown in Figure 4b can be used to determine the values p_1 and p_2 in equation (19). The results indicate values of approximately 11.11 and 8.45×10^{-3} $\mathrm{m^1\,Hz^2\,V^{-1}}$, for p_1 and p_2, respectively, for a model of 19 discrete frequency modes. This corresponds to $\tau_c = 25$ hours for a system with 19 modes each with a wave mode amplitude of $A = 49$ μV m^{-1}, and implies a value of $\tau_c < 25$ hours for larger wave amplitudes. The values shown for p_1 and p_2 in Figure 4c are not used further in the analysis presented here since we only consider systems with 19 wave modes.

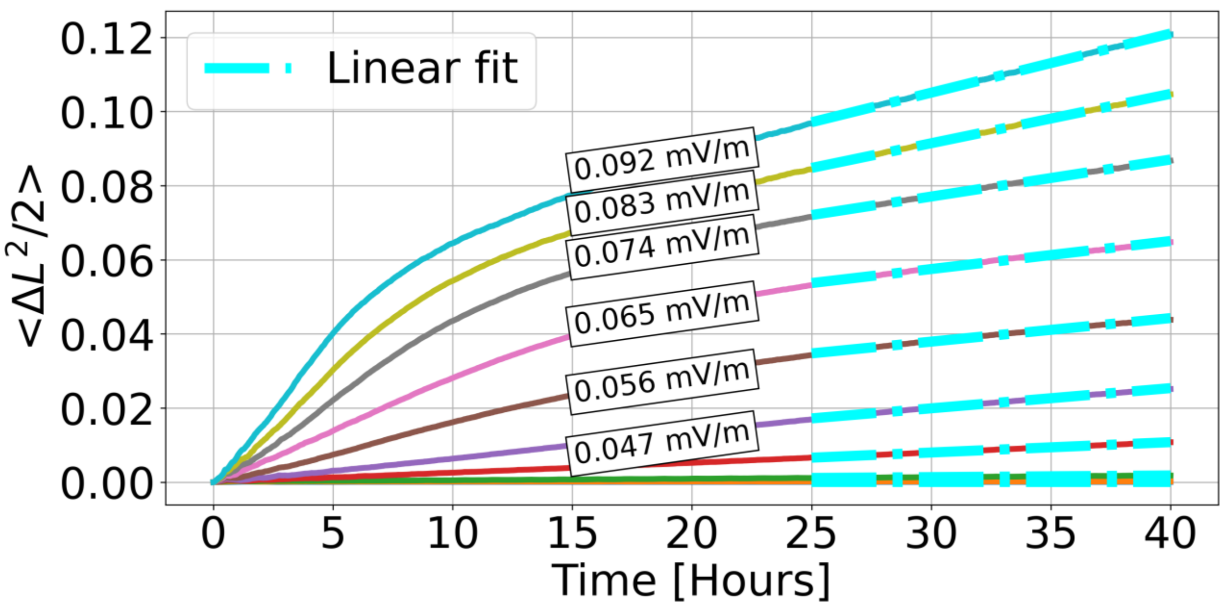

Figure 5. $\langle \Delta L^2/2 \rangle$ as a function of time, for a range of wave mode amplitudes A. This plot illustrates the fitting of the ensemble linear function of $\langle \Delta L^2/2 \rangle$ as a function of time for a range of simulation runs and demonstrates the method for estimating the diffusion coefficient D_{LL} for a given wave amplitude A. The fitting region is determined by the CDT τ_c, with the numerical results suggesting that $\tau_c \leq 25$ hours for $A \geq 0.049$ mV/m.

Finally, the radial diffusion coefficient which characterizes the later time stochastic evolution in our model is calculated through equation (14) by applying a linear fit on the later times of $\langle \Delta L^2 \rangle$ as a function of time, and where the slope corresponds directly to $2 \times D_{LL}$ (see Figure 5). Furthermore, by simulating multiple simulation runs using different wave amplitudes, the D_{LL} can be parameterized in terms of A, and consequentially, wave PSD.

6 Rates of Radial Diffusion: Results

Here the results obtained from our wave-particle simulation model are tested against the analytical D_{LL} equation for electric field disturbances in a symmetric background dipole field defined by (e.g., Fei et a., 2006; Lejosne, 2019)):

$$D_{LL}^E = \frac{L^6}{8R_E^2 B_{Eq}^2} \sum_m P_m^E(m\omega_d) \, , \#(20)$$

where the summation over m in P_m^E is used to take account of the wave electric field PSD at the drift resonance frequencies where wave angular frequency $\omega = m\omega_d$. Given our model only contains wave modes with a single value of $m = 20$, the summation is reduced to only one azimuthal harmonic of the azimuthal electric field power spectral density given by P_{20}^E.

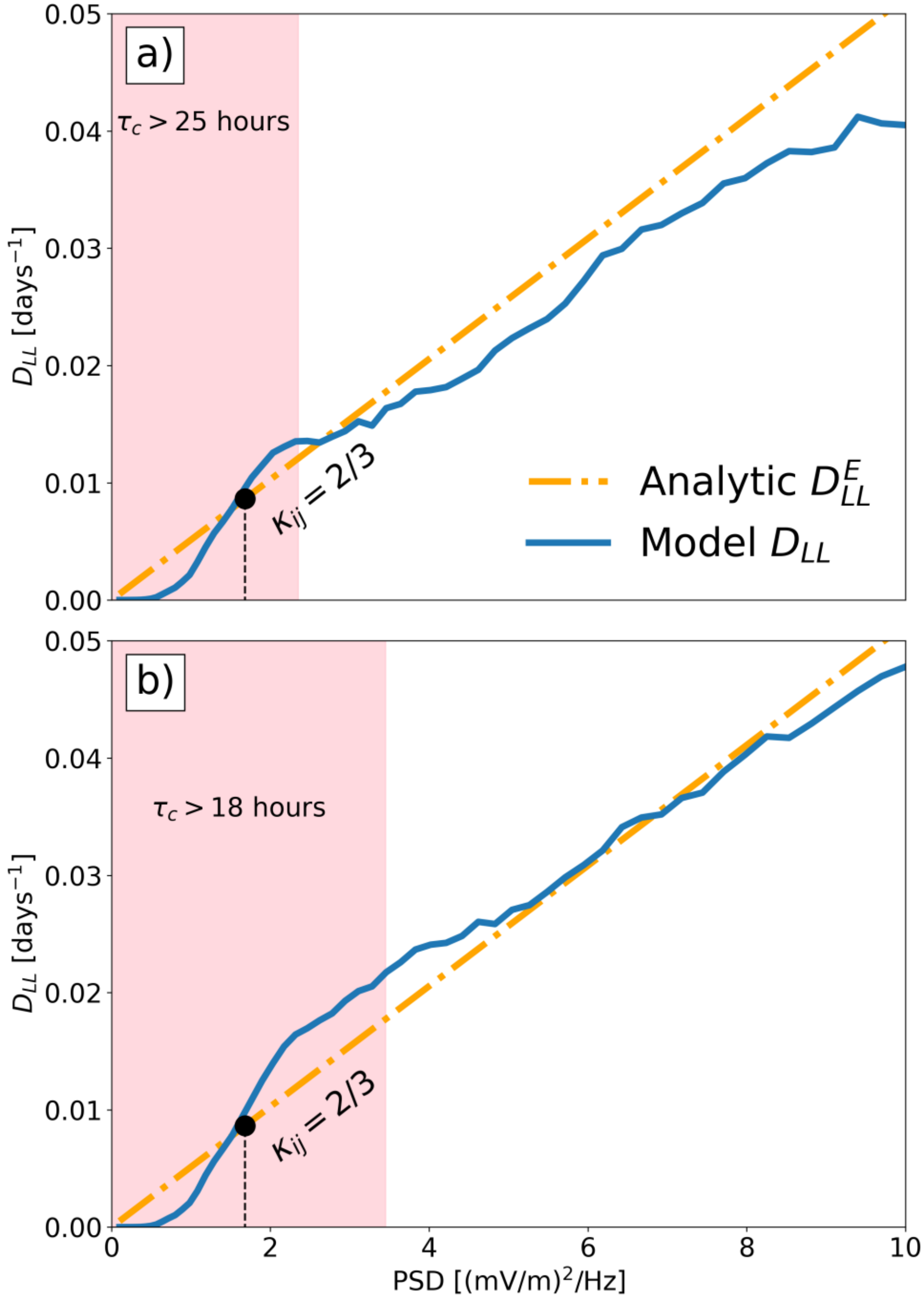

Figure 6. D_{LL} as a function of PSD. Panel (a) The blue line shows D_{LL} as a function of wave PSD, derived from linear fits of $\langle \Delta L^2 \rangle$ in time from 25 to 40 hours. The red shaded region represents the range of wave PSDs for which the dynamical system requires more than 25 hours to reach the CDT, τ_c, therefore introducing errors into the D_{LL} estimates in that region. Panel (b) is identical to panel (a), except that the fits of $\langle \Delta L^2 \rangle$ in time are taken from 18 to 33 hours. This increases the range of PSD magnitudes for which τ_c lies within this time interval, and where the fits can be expected to have errors, indicated by the expanded red shaded region of PSD where this occurs. In both panels the dashed orange line shows the results from the analytic expression for D_{LL} from equation (20) and calculated at $L = 5.158$. This value of L was chosen since our simulation domain spans from $L = 4$ to $L = 6$ with an average value $L^6 = 5.158^6$ (since

equation (20) is proportional to L^6). Finally, the vertical dashed line shows the location of the transition to diffusive behavior based on the two-thirds overlap criteria satisfied by all adjacent resonance islands where the discrete frequency wave modes pairs are separated by Δf.

Figure 6 shows the evolution of D_{LL} measured in our model by using fits of $\langle \Delta L^2 \rangle$ as a function of time from simulation runs (blue curves) and parametrized in terms of wave PSD. By running simulations with a range of wave amplitudes, we are able to study the particle ensemble dynamics before and after the two-thirds criterion during a finite duration of simulation time. This criterion is picked at the lowest amplitude required for the entire simulation domain to satisfy equation (11), as shown in Figure 3a. As shown in both Figures 6a and 6b, the regions before and after the two-thirds criterion are satisfied demonstrate clear differences in the particle ensembles' behavior. When in the former region and close to the origin, it is evident that the wave-particle dynamics are localized and produce very little net transport within the particle ensemble ($D_{LL} \approx 0$). However, as the PSDs approach the values required to exceed the two-thirds overlap criterion, the sudden growth of D_{LL} is indicative of the onset of net particle transport in the entire system (see Figure S1 of Supporting Information).

As the wave amplitude increases, the adjacent resonant islands begin to merge, and through the satisfaction of the two-thirds criterion for a set of discrete frequency modes with a spectrum of a comb of uniform spacing Δf, the entire resonant domain (with exception of very small regions of phase space near the center of the resonant islands) established by the frequency spectrum becomes accessible to the particles and where they can undergo stochastic, diffusive, transport. Since the particles need to evolve beyond the CDT to become decorrelated, we can conclude that the wave-particle dynamics can only become stochastic on timescales $t > \tau_c(A, \Delta f)$. However, it is also important to note that these small remnant and persisting resonant islands prevent the entire phase space from behaving diffusively. Hence the overall rates of diffusive particle transport induced through resonant wave-particle interaction of the entire ensemble within our simulations should be slightly less than the rates of D_{LL}^E predicted by analytic radial diffusion theory such as that shown in equation (20). In both Figure 6a and 6b, where the D_{LL} is calculated over the entire ensemble from the particle simulations (blue lines), the periodic dynamics caused by particles within the resonant islands can explain which the model-derived D_{LL} (blue line) is typically slightly less than the theoretical prediction (yellow line). This effect is more prominently in Figure 6a, when the system is analyzed on timescales $t > \tau_c$, and where the D_{LL} estimate obtained from our particle-tracing model simulation runs (blue line) lies immediately below the estimate from equation (20) (yellow line).

In addition, it is also clear in Figure 6 that the onset of net particle transports within the entire domain does not immediately imply full stochasticity. In both Figure 6a and 6b, near but after the two-thirds overlap criterion is satisfied (vertical dashed line), the estimate of D_{LL} derived from our simulation runs is higher than that predicted by the analytic model in equation (20). Given that the method used to determine D_{LL} assumes stochasticity a priori, we may suspect that the system in this narrow region may not yet be completely stochastic. Further, for the range of PSDs where the CDT is satisfied (PSD > 2.4 $mV^2\ m^{-2}\ Hz^{-1}$ for Figure 6a, and PSD > 3.5 $mV^2\ m^{-2}\ Hz^{-1}$ for 6b), the simulation results are consistent with the analytic estimate from equation (20). Only when the system has evolved for long enough for decorrelation to occur, as well as being set up such the resonant islands are sufficiently close that they satisfy the two-thirds overlap criteria, is it reasonable to assert that the system is behaving stochastically.

In both Figure 6a and 6b, the ensemble dynamics appear to display a faster transport than predicted by radial diffusion theory in the region where the CDT is not satisfied during the duration of simulation time used in the model runs. This result is artificial since the linear fit mechanism being used to assess D_{LL} is not applicable in such region, but the transport rate in any case, is faster than that of stochastic diffusion. With our wave model, the two-thirds resonance island criterion is satisfied at $A \approx 41\,\mu\mathrm{V/m}$ or PSD $\approx 1.68\,\mathrm{mV^2m^{-2}Hz^{-1}}$ for $\Delta f = 0.5\,\mathrm{mHz}$. This means the CDT needed to solve the transition to diffusion requires a minimum time of $\tau_c \approx 40$ hours given the parameters used in Figure 4b (and further additional hours needed in order to assess the stochastic transport rate). Due to many computational and modeling constraints (e.g., computational resources, too many particles removed from the system etc.), we were not able to produce any results where the two-thirds resonance island overlap criterion was always satisfied after the CDT. Nonetheless, careful considerations for the CDT are needed when analyzing the results using statistical models. Lastly, these results also suggest the importance of the small regions of regular dynamics within small remnant resonant islands that may remain in the phase space, even if the majority of the phase space now lies within a stochastic regime. During the transition, the fraction of the phase space occupied by such regions becomes smaller as the system continues its transition towards more stochasticity – as shown clearly in Figure 2. For radial diffusion, a theory foundationally based on the effects of resonant wave-particle interactions, and especially for parameters which place the system close to the transition region, some fraction of the phase space may still lie within small regions of remnant resonant islands that still undergo no net particle transport over long timescales.

7 Conclusions

In this work, we used a particle-tracing simulation model to examine the dynamics of ultra-low frequency (ULF) wave-particle interactions with an ensemble of relativistic outer radiation belt electrons. We used a simplified model appropriate for examining the dynamics of equatorially mirroring electrons in a dipole magnetic field, and where the waves are assumed to the Alfvenic and in the fundamental field-guided harmonic mode such that the equatorially mirroring electron dynamics are only under the influence of electric field perturbations. We further examined the ensemble electron dynamics as a result of resonant interactions with multiple discrete frequency wave modes, with a spectrum with a comb of uniformly separated frequencies spanning a fixed frequency range and a single azimuthal mode number. The resulting electron dynamics in response to these multiple discrete frequency modes are simulated in narrow range of L-shells, and the results analyzed in the time domain including: assessing the time for the temporal dynamics to become stochastic, beyond a correlation decay time τ_c (CDT); deriving an expression for the (CDT) for this system, including through comparison to the dynamics of a kicked rotator system; assessing the rates of radial diffusion, and comparing then to analytical expressions for the radial diffusion coefficient D_{LL}; and defining and validating an expression for the timescale for the transition to stochastic radial diffusion through an application of a generalization of the two-thirds resonance island overlap condition. The major results arising from this analysis can be summarized by the following points:

1. The degree of coherence in the resonant interactions of simulated electrons subjected to multiple discrete frequency wave perturbations demonstrates a dependence on both the wave frequency separation and the amplitude of the perturbing electric field strength. These effects can be combined into expressions for the primary resonant island separation and island width in the electron's phase space. Further, the utilization of stroboscopic

maps visualized these underlying phase space structures and verified the principles of the two-thirds resonant island overlap criterion as a predictor of the transition to stochastic dynamics and which is commonly referenced in statistical theory (e.g., Lichtenberg & Lieberman, 1992). Qualitatively, there is a distinct difference between coherent and diffusive systems (see Figure 2). We used the two-thirds resonance island overlap criterion to quantify the transition to diffusion, and along with it, derived the relevant parameters required for equation (11) which presents an analytic expression for the criteria for the transition to diffusion.

2. A comparison between the analytical formulation of D_{LL} (equation (20)) and the ensemble particle transport validated that the model produced the expected rates of diffusion transport during later times, and that the transition to this transport can be predicted using the two-thirds resonance island overlap condition. Further, close to the point of resonance island overlap (e.g., because the wave amplitude becomes sufficiently large for a given resonance island separation), the simulations often showed some modulations in the ensemble rates of radial transport as a function of wave PSD which were superimposed on top of a smooth transition from near-zero net rates of transport at early times to those characteristics of diffusion at later times. We showed that, whilst the two-thirds criterion led to an accurate prediction of time of the onset of net ensemble particle transport, it is additionally only after the system had become sufficiently decorrelated, beyond the system's inherent CDT, that the particle transport process become stochastic. It is only beyond this time that transport rates can be described using analytic radial diffusion coefficients. This is illustrated in Figures 6a and 6b, where the ensemble dynamics can locally undergo rates of transport which are faster than radial diffusion when only the two-thirds overlap criterion is satisfied. However, at even later times (for fixed wave amplitudes), the transport rates then behave in line with the expected stochastic rates of radial diffusion when both conditions are met. Additionally, through the use of a particle-tracing model, we showed (as expected) that even in the stochastic regime, there can still be small and contracted regions in the phase space, which are the remnants of the resonance islands, where particle motion remains periodic and produce no net particle transport. These dynamics are due to the fact that some particles remain trapped within these small remnant resonant islands of a given resonant wave mode. Although small, they can introduce small corrections to the overall ensemble rates of radial diffusion as compared to analytic expressions for transport rates which exclude such effects.

3. The distinct transition in the ensemble transport rates from early to later times, for example as revealed in the behavior of $\langle \Delta L^2 \rangle$ as a function of time shown in Figure 4a, are clearly indicative of the importance of a finite system correlation decay time in the transition to stochastic behavior. This can be attributed to the timescale required for a dynamical system to undergo sufficient phase mixing to achieve this decorrelation. This effect is often ignored in assessments of the radial diffusion of relativistic electrons in the radiation belts, However, its impacts are significant and for realistic values of wave parameters the timescale for this transition to stochasticity can be quite long. For example, in the particle-tracing simulations (see Figure 4), using parameters representative of the ULF waves in the magnetosphere, and for modes which are relatively closely spaced in frequency, this decorrelation timescale can be several hours. That would mean that if such a situation was repeated in the magnetosphere, the waves

and the wave-particle interactions would need to persist for hours before the transport rates can be estimated using a radial diffusion paradigm. This is important since it suggests that early time dynamics might not be able to be described diffusively (see also, for example, the discussion in Mann et al., 2012; see also Ukhorskiy & Sitnov, 2012). The duration of the correlation decay process revealed here is a fundamentally important caveat for using the radial diffusion paradigm for radiation belt modeling and assessing the rates of radial transport in the radiation belts. In systems where the particle's guiding center drift equations are governed by first order coupled differential equations (e.g., this model), the difference between an ordered and de-correlated state is purely determined by the ensemble characteristics of the particles' position. Moreover, these positions are uniquely determined by the ULF wave power spectra and other pertaining characteristics, and only after the motion of the particles has transformed the system into a de-correlated state, can the entire ensemble behave diffusively. Significantly, it is only after this CDT can the radiation belt electrons be characterized using a radial diffusion coefficient. Additionally, the wave fields themselves must also be such to additionally satisfy the two-thirds resonance island overlap criterion in order for the ensemble particle motion to be able to behave diffusively and to be transported through the entire phase space, rather than either being trapped inside individual resonance islands or experience periodic advection in the regions outside the resonance islands. Similarly, as discussed by Ukhorskiy et al., (2006) and Ukhorskiy & Sitnov, 2012, if the structure of the background magnetosphere is also being changed on the timescales of the ensemble correlation decay time, this may also affect the ability of the system to attain the required decorrelated state in order to transition to stochastic radial diffusion.

Our results have fundamental implications for understanding radiation belt electron dynamics. Not least because when the CDT is long, radiation belt transport on the timescales of the perturbing ULF wave packets observed in the magnetosphere may not be diffusive. In such cases, transport rates should not be estimated using the diffusive paradigm. As we show, the CDT for the simulation model presented here depends strongly on the mode frequency spacing Δf as well as wave amplitude – shorter CDTs for larger wave amplitudes and closer frequency spacing. However, if fast transport occurs due to short-lived bursts of short wavetrain ULF wave modes with a small number of discrete frequencies, then even if they have large amplitude the overall radial transport may be more likely to be coherent than diffusive (cf. Mann et al., 2012). The model we examined here presents a mechanism for assessing whether the wave amplitudes are large enough and the Δf small enough for the transport to be described as diffusive, and the timescales of interaction which are required in order for the system to decorrelate and transition to stochastic diffusion.

Similarly, in the presence of electron phase space densities which increase with L-shell, non-diffusive resonance island dynamics can result in the coherent inward transport of regions of large electron phase space density. As shown by Degeling et al. (2008), if the waves decay on the timescales of the transport around discrete resonance islands, those regions of phase space with enhanced electron phase space density at higher L can be coherently transported into the inner magnetosphere and will remain there leaving regions of large electron flux in the inner magnetosphere once the ULF waves have decayed. Such transport is coherent and not diffusive. Conversely, many modes, with sufficiently close frequency spacing, Δf, even if they are of small amplitude, can result in diffusive transport on sufficiently long timescales.

Overall, the relative contributions arising from coherent and diffusive transport for electron dynamics in the radiation belts remains relatively poorly understood. The model framework which we present here presents a series of tools which can be used to assess this, depending on wave amplitude and the characteristics of the wave spectra. This includes not only an assessment of whether the resonant islands are sufficiently close for their overlap to lead to a transition which enables long distance transport in phase space, but also an assessment of the timescales required in order for the system to transition to stochasticity. It is only after such times that the transport rates can be accurately estimated using a radial diffusion paradigm.

Appendix A: Resonant Island Center Derivation

The primary resonant island is centered on a L-value where the resonance condition is satisfied. Using equations (2) and (4) and for electric fields with no DC component so that its contribution is zero over the average of 1 wave cycle, we can neglect the first term in equation (2):

$$\dot{\phi}^2 \approx \frac{9\mu m_e c^2}{2q^2 R_E^4 B_0 L}\left[1+\frac{m_e c^2 L^3}{2\mu B_0}\right]^{-1} . \#(\mathrm{A1})$$

Further, we can invoke the resonance condition, equation (10):

$$\left(\frac{\omega}{m}\right)^2 \approx \frac{9\mu m_e c^2}{2q^2 R_E^4 B_0 L}\left[1+\frac{L^3 m_e c^2}{2\mu B_0}\right]^{-1} . \#(\mathrm{A2})$$

The right-hand side of equation (A2) is of the form $(1+x)^{-1}$. For high energies where γ can be approximated by its first order Taylor expansion, $x \ll 1$, the right-hand side term can be expanded. Rewriting, we obtain a cubic polynomial:

$$L^3 + \left(\frac{\omega}{m}\right)^2 \left(\frac{2qR_E^2 B_0}{3m_e c^2}\right)^2 L - \frac{2\mu B_0}{m_e c^2} \approx 0 . \#(\mathrm{A3})$$

Equation (A3) is in the form of a depressed cubic. In such a case, we can invoke Cardano's formula, giving us the solution of only 1 real root, which approximates the resonant island center, equation (12).

Appendix B: Resonant Island Half-Width Derivation

Following a similar derivation found in Degeling et al. (2007), the primary resonant island half-width can be estimated for particle dynamics in a symmetric dipole field subjected to a resonant monochromatic wave oscillation mode. The center of the primary resonant island is dictated by the resonance condition. Again, under the approximation for high energies, the Lorentz factor can be approximated by its first order expansion

$$\frac{1}{\gamma} \approx \sqrt{\frac{L^3 m_e c^2}{2\mu B_0}}\left[1-\frac{L^3 m_e c^2}{4\mu B_0}\right] . \#(\mathrm{B1})$$

At these energies, the electron's azimuthal motion is primarily driven by *gradient* drift, and the radial motion is solely driven by *E-cross-B* drift. For small amplitude perturbations, the resonant island spans a small range in L, and $E_0(L_0)$ can be regarded as approximately constant across the entire width of the island. By defining the wave phase as $\psi = m\phi - \omega t$, the electrons' equations of motions can be then approximated:

$$\begin{cases} \dot{L} = \dfrac{E_0(L_0)}{R_E B_0} L^3 \cos(\psi) \\ \dot{\phi} \approx -\dfrac{1}{q}\sqrt{\dfrac{9\mu m_e c^2}{2R_E^4 B_0}}\left[L^{-\frac{1}{2}} - \dfrac{m_e c^2}{4\mu B_0} L^{\frac{5}{2}}\right] \end{cases} . \#(\text{B2})$$

Here, we drop the ζ factor from equation (9) for simplicity since the variations in L is small given small perturbations. Furthermore, $\dot{L}$ can be expanded using the chain rule, and $\dot{\psi}$ can be expanded in L near the resonance L_0:

$$\dot{L} = \frac{\partial L}{\partial \psi}\dot{\psi}; \qquad \dot{\psi} \approx \dot{\psi}(L_0) + (L - L_0)\left.\frac{\partial \dot{\psi}}{\partial L}\right|_{L=L_0}, \#(\text{B3})$$

where $\dot{\psi}(L_0) = 0$ is given by the resonance condition. One can see that $\dot{\psi} \approx (L - L_0) m \left.\frac{\partial \dot{\phi}}{\partial L}\right|_{L=L_0}$ which gives:

$$\frac{\partial L}{\partial \psi} = \frac{E_0(L_0) L^3}{R_E B_0}\cos(\psi)\frac{1}{(L - L_0) m \left.\dfrac{\partial \dot{\phi}}{\partial L}\right|_{L_0}} . \#(\text{B4})$$

Equation (B4) is separable and can be integrated over the outermost island shell. However, for small perturbation amplitudes, we can assume the resonant island half-width is symmetric, allowing us to only evaluate the half-width on one side:

$$\int_{L_0}^{L_0+\delta L} \frac{(L - L_0)}{L^3} dL = \frac{E_0(L_0)}{R_E B_0 m \left.\dfrac{\partial \dot{\phi}}{\partial L}\right|_{L_0}} \int_0^{\frac{\pi}{2}} \cos(\psi) d\psi . \#(\text{B5})$$

Finally, small wave amplitudes allow for the approximation: $L_0 \gg \delta L$, and evaluating $\left.\frac{\partial \dot{\phi}}{\partial L}\right|_{L_0}$, we can approximate the primary resonant island half-width:

$$\delta L \approx \left(\frac{32 q^2 R_E^2}{9 B_0 \mu m_e c^2}\right)^{\frac{1}{4}} \sqrt{\frac{E_0(L_0)}{m}\frac{L_0^{4.5}}{1 + \dfrac{5 m_e c^2}{4\mu B_0} L_0^3}} . \#(\text{B6})$$

Appendix C: *K* Proportionality Derivation

Following from equation (1) and (2) which describes the equatorial motion of a charged particle under the influence of electromagnetic fields, and assuming that the azimuthal motion is purely driven by *gradient* drift, we can express $\dot{\phi}$ by its approximation found in equation (A1). The charged particle's equations of motion in our near-integrable system of 19 modes can be expressed as:

$$\begin{cases} \dot{L} = \dfrac{A}{R_E B_0} L^3 \displaystyle\sum_{n=75}^{93} \cos(m\phi - n\Delta\omega t) \\ \dot{\phi} = \omega_d(L) \approx -\dfrac{1}{q}\sqrt{\dfrac{9\mu m_e c^2}{2R_E^4 B_0 L}}\left[1 + \dfrac{m_e c^2 L^3}{2\mu B_0}\right]^{-1/2} \end{cases}, \#(C1)$$

Where $\Delta\omega$ is determined by the frequency separation of our perturbations, $\Delta\omega = 2\pi\Delta f$, and the index from 75 to 93 corresponds to our frequency range from 37.5 mHz and 46.5 mHz. In equation (C1), for simplicity, we used a flat amplitude profile in L, $E_0(L) = A,$ and electric wave disturbance with no extra phase factors. Additionally, we use a change of variables given by $I = L^{-2}$, and further break down the azimuthal motion by its first-order Taylor expansion in I near the vicinity of our simulation domain, giving us:

$$\begin{cases} \Delta\dot{I} = -2\dfrac{A}{R_E B_0} \displaystyle\sum_{n=75}^{93} \cos(m\phi - n\Delta\omega t) \\ \dot{\phi} \approx \omega_d(I_0) + \omega_d'(I_0)\Delta I \end{cases}. \#(C2)$$

Following a series of substitutions, as similarly done in Ukhorskiy & Sitnov (2012):

$$\Delta\omega t \to mt', \qquad \frac{m^2}{\Delta\omega}\omega_d'(I_0)\Delta I \to I, \qquad \text{and} \qquad \theta = m\phi - m\omega_d(I_0)t, \#(C3)$$

and removing the prime notation on time, $t' \to t$, we can describe our dynamical system with the new equations of motion:

$$\begin{cases} \dot{I} = -2\dfrac{A}{R_E B_0}\dfrac{m^3}{(\Delta\omega)^2}\omega_d'(I_0) \displaystyle\sum_{n=75}^{93} \cos\left(\theta - \left[nm - \frac{m^2\omega_d(I_0)}{\Delta\omega}\right]t\right) \\ \dot{\theta} = I \end{cases}. \#(C5)$$

The argument of cosine can be further decomposed using the resonance condition, $\omega = m\omega_d$, where ω is the resonant frequency for a particle situated on $I_0 = L_0^{-2}$. Since we expanded $\dot{\phi}$ near the vicinity of a resonance in our simulation domain, the resonant frequency at I_0 is given by $m\omega_d(I_0)$ which is contained in 1 of the terms found in the summation. That is, we can rewrite as $\omega = n_R\Delta\omega$, where n_R is the index of the summation that corresponds to the resonant frequency of the particle at I_0, and $75 \le n_R \le 93$. We can now rewrite our index such that:

$$m(75 - n_R) = i, \qquad \text{and} \qquad m(93 - n_r) = k,$$

where the azimuthal wavenumber m and n_R are integers, and i and k are now our new indices for the summation increasing in increments of m. Rewriting our equations of motion:

$$\begin{cases} \dot{I} = -2\dfrac{A}{R_E B_0}\dfrac{m^3}{(\Delta\omega)^2}\omega_d'(I_0) \displaystyle\sum_{\substack{n=i,i+m,\\ i+2m,\dots}}^{k} \cos(\theta - nt) \\ \dot{\theta} = I \end{cases}, \#(C6)$$

equation (C6) becomes reminiscent of a kicked-rotator system which is given by:

$$\begin{cases} \dot{I} = \dfrac{K}{4\pi^2} \displaystyle\sum_{n=-\infty}^{\infty} \cos(\theta - nt) \\ \dot{\theta} = I \end{cases} . \#(C7)$$

Here, K in equation (C7) is indeed the non-linearity parameter we are after, and by direct comparison with equation (C6), we can deduce that $K = 8\pi^2 A m^3 \omega_d'(I_0)/R_E B_0\,(\Delta\omega)^2$ is the non-linearity parameter for our simplified dynamical system. It follows that the approximate proportionality of the non-linearity parameter our system and similar systems is given by: $K \propto A/\Delta f^2$. This approach provides us with an ansatz which we can test using the numerical results from the wave-particle interaction simulations presented here.

Acknowledgments

This work is generously supported by the Canadian NSERC Undergraduate Summer Research Award (Grant #: 540714 – 2019 and 563198 – 2021). This work was also supported by funding from a Canadian NSERC Discovery Grant to IRM. AD acknowledges support from the National Natural Science Foundation of China (Grant #: 41774172). ZGL would like to thank IRM and LGO for taking him on this research project during his undergraduate degree, and thanks Compute Canada for computation resources.

Open Research

The model simulation results used in this study are available online (https://doi.org/10.5281/zenodo.10645257).

References

Baker, D. N. (2000), The occurrence of operational anomalies in spacecraft and their relationship to space weather, *IEEE Trans. Plasma Sci.*, **28**, 2007–2016, doi:10.1109/27.902228.

Beutier, T., & Boscher, D. (1995). A three-dimensional analysis of the electron radiation belt by the Salammbô code. *Journal of Geophysical Research*, **100**(A8), 14853. https://doi.org/10.1029/94JA03066

Birmingham, T. J., Northrop, T. G., and Fälthammar, C.-G. (1967), Charged particle diffusion by violation of the third adiabatic invariant, *The Physics of Fluids*, **10**, 2389–2398, doi: 10.1063/1.1762048

Chirikov, B. V., A universal instability of many-dimensional oscillator systems, *Phys. Rep.*, *52*, 263, 1979.

Davis, L., & Chang, D. B. (1962). On the effect of geomagnetic fluctuations on trapped particles. *Journal of Geophysical Research*, **67**(6), 2169–2179. https://doi.org/10.1029/JZ067i006p02169

Degeling, A. W., Ozeke, L. G., Rankin, R., Mann, I. R., and Kabin, K. (2008), Drift resonant generation of peaked relativistic electron distributions by Pc 5 ULF waves, *J. Geophys. Res.*, ***113***(A2), A02208, doi:10.1029/2007JA012411.

Degeling, A. W., Rankin, R., & Elkington, S. R. (2011). Convective and diffusive ULF wave driven radiation belt electron transport. *Journal of Geophysical Research*, **116**, A12217. https://doi.org/10.1029/2011JA016896

Degeling, A., Rankin, R., Kabin, K., Marchand, R., & Mann, I. (2007). The effect of ULF compressional modes and field line resonances on relativistic electron dynamics. *Planetary and Space Science*, **55**(6), 731–742. https://doi.org/10.1016/j.pss.2006.04.039

Degeling, A. W., Rankin, R., Wang, Y., Shi, Q. Q., & Zong, Q. G. (2019). Alteration of particle drift resonance dynamics near poloidal mode field line resonance structures. *Journal of Geophysical Research: Space Physics*, **124**(9), 7385–7401. https://doi.org/10.1029/2019JA026946

Elkington, S. R., Hudson, M. K., & Chan, A. A. (1999). Acceleration of relativistic electrons via drift-resonant interaction with toroidal-mode Pc-5 ULF oscillations. *Geophysical Research Letters*, **26**(21), 3273–3276. https://doi.org/10.1029/1999GL003659

Elkington, S. R., Hudson, M. K., & Chan, A. A. (2003). Resonant acceleration and diffusion of outer zone electrons in an asymmetric geomagnetic field. *Journal of Geophysical Research*, **108**(A3), 1116. https://doi.org/10.1029/2001JA009202

Fälthammar, C.-G. (1965). Effects of time-dependent electric fields on geomagnetically trapped radiation. *Journal of Geophysical Research*, **70**(11), 2503–2516. https://doi.org/10.1029/JZ070i011p02503

Fälthammar, C.-G. (1968). Radial diffusion by violation of the third adiabatic invariant. In B. M. McCormac (Ed.), *Earth's Particles and Fields*. Reinhold, New York: NATO Advanced Study Institute.

Fei, Y., Chan, A. A., Elkington, S. R., & Wiltberger, M. J. (2006). Radial diffusion and MHD particle simulations of relativistic electron transport by ULF waves in the September 1998 storm. *Journal of Geophysical Research*, 111, A12209. https://doi.org/10.1029/2005JA011211

Goldstein, H., Poole, C., Safko, J. (2002). *Classical Mechanics*. American Association of Physics Teachers.

Horne, R. B., Glauert, S. A., Meredith, N. P., Koskinen, H., Vainio, R., Afanasiev, A., et al. (2013). Forecasting the Earth's radiation belts and modelling solar energetic particle events: Recent results from spacecast. *Journal of Space Weather and Space Climate*, **3**, A20. https://doi.org/10.1051/swsc/2013042

Kellogg, P. J. (1959). Van Allen radiation of solar origin. *Nature,183*, 1295.

Lejosne, S. (2019). Analytic expressions for radial diffusion. *Journal of Geophysical Research: Space Physics*, **124**, 4278–4294. https://doi.org/10.1029/2019JA026786

Lichtenberg, A. J., & Lieberman, M. A. (1992). *Regular and chaotic dynamics* (Vol. 38). Springer Science & Business Media.

Loto'aniu, T. M., Mann, I. R., Ozeke, L. G., Chan, A. A., Dent, Z. C., & Milling, D. K. (2006). Radial diffusion of relativistic electrons into the radiation belt slot region during the 2003 halloween geomagnetic storms. *Journal of Geophysical Research*, **111**(A4). https://doi.org/10.1029/2005JA011355

Mann, I. R., Murphy, K. R., Ozeke, L. G., Rae, I. J., Milling, D. K., Kale, A. A., & Honary, F. F. (2012). The role of ultralow frequency waves in radiation belt dynamics. *Geophysical Monograph Series*, **199**, 69–91.

McIlwain, C. E. (1961). Coordinates for mapping the distribution of magnetically trapped particles. *Journal of Geophysical Research*, **66**(11),3681–3691. https://doi.org/10.1029/JZ066i011p03681

Northrop, T. G. (1963). Adiabatic charged-particle motion. *Reviews of Geophysics*, **1**(3), 283–304.

Parker, E. N. (1960). Geomagnetic fluctuations and the form of the outer zone of the Van Allen radiation belt. *Journal of Geophysical Research*, **65**(10), 3117–3130. https://doi.org/10.1029/JZ065i010p03117

Reeves, G. D., Chen, Y., Cunningham, G. S., Friedel, R. W. H., Henderson, M. G., Jordanova, V. K., Koller, J., Morley, S. K., Thomsen, M. F., & Zaharia, S. (2012). Dynamic Radiation Environment Assimilation Model: DREAM. *Space Weather*, **10**, S03006. https://doi.org/10.1029/2011SW000729

Riley, P., & Wolf, R. A. (1992). Comparison of diffusion and particle drift descriptions of radial transport in the Earths inner magnetosphere. *Journal of Geophysical Research*, **97**(A11), 16865. https://doi.org/10.1029/92JA01538

Schulz, M., & Lanzerotti, L. J. (1974). *Particle Diffusion in the Radiation Belts* (Vol. **7**). Verlag, Berlin, Heidelberg: Springer.

Southwood, D. (1974). Some features of field line resonances in the magnetosphere. *Planetary and Space Science*, **22**(3), 483 - 491. https://doi.org/10.1016/0032-0633(74)90078-6

Southwood, D. J., Dungey, J. W., & Etherington, R. J. (1969). Bounce resonant interactions between pulsations and trapped particles. *Planetary and Space Science*, **17**(3), 349–361. https://doi.org/10.1016/0032-0633(69)90068-3

Subbotin, D. A., & Shprits, Y. Y. (2009). Three-dimensional modeling of the radiation belts using the Versatile Electron Radiation Belt (VERB) code. *Space Weather*, **7**, S10001. https://doi.org/10.1029/2008SW000452

Ukhorskiy, A. Y., Anderson, B. J., Takahashi, K., & Tsyganenko, N. A. (2006). Impact of ULF oscillations in solar wind dynamic pressure on the outer radiation belt electrons. *Geophysical Research Letters*, **33**, L06111. https://doi.org/10.1029/2005GL024380

Ukhorskiy, A. Y., & Sitnov, M. I. (2012). Dynamics of radiation belt particles. *Space Science Reviews*, **179**, 545–578. https://doi.org/10.1007/s11214-012-9938-5

Welch, P. (1968), The use of fast Fourier transform for the estimation of power spectra: A method based on time averaging over short, modified periodograms, *IEEE Transactions on Audio and Electroacoustics*, **15**(2), 70-73, doi: 10.1109/TAU.1967.1161901

Xiang, Z., Tu, W., Li, X., Ni, B., Morley, S. K., & Baker, D. N. (2017). Understanding the mechanisms of radiation belt dropouts observed by Van Allen Probes. *Journal of Geophysical Research: Space Physics*, **122**(10), 9858–9879. https://doi.org/10.1002/2017JA024487

Zaslavsky, G.M. (2002), Chaos, fractional kinetics, and anomalous transport. *Phys. Rep*. **371**, 461